16th World Conference on Earthquake, 16WCEE 2017

Santiago Chile, January 9th to 13th 2017

Paper N° 3858

Registration Code: S-J1464284622

SEISMIC DEMAND ON PILES IN SITES PRONE TO LIQUEFACTION-INDUCED LATERAL SPREADING

C. Barrueto(1), E. Sáez(2,3) & C. Ledezma(2,3)

(1) *MSc Student, Department of Structural and Geotechnical Engineering, Pontificia Universidad Católica de Chile, cgbarrue@uc.cl*
(2) *Professor, Department of Structural and Geotechnical Engineering, Pontificia Universidad Católica de Chile, esaez@ing.puc.cl ; ledezma@ing.puc.cl*
(3) *Researcher, Center for Integrated Natural Disaster Management CONICYT/FONDAP/15110017, Chile.*

Abstract

Lateral spreading is one of the most important effects of liquefaction because it can cause significant ground deformation and damage to existing infrastructure. In 2010, the Lo Rojas fishermen port in Coronel, southern Chile, was affected by this phenomenon due to the Mw 8.8 Maule earthquake. To identify and to model the soil layers at Lo Rojas fishermen port, the geotechnical model developed by [4] was used. This soil profile was obtained through an extensive field survey, including SPTs and CPTs soundings, and the application of geophysical surface techniques. The mechanical characterization of the soil layers at the site was performed by laboratory tests of the materials extracted during the exploration phase, including monotonic and cyclic triaxial tests, and resonant column experiments. With the obtained laboratory curves and the literature data, constitutive models for each soil layer were calibrated and used on a finite-element model on Plaxis® software. To properly reproduce the experimental behavior of the liquefiable soil layer, the UBC3D-PLM model was used. The results of this study will improve the understanding of the seismic demand on piles due to lateral spreading.

Keywords: lateral spreading; laboratory testing; finite element modeling; Plaxis®; UBC3D-PLM model

1. Introduction

The Mw 8.8 earthquake of 2010 affected Chilean infrastructure, and it caused important destruction in the central zone of the country. Many buildings and ports near the epicenter zone were severely damaged due to ground failure and lateral spreading as described in [3, 5].

This paper focuses on the study of the Lo Rojas fishermen port in Coronel, Bío-Bío Region, where liquefaction-induced lateral spreading significantly damaged the existing pier. A post-earthquake survey determined cumulative ground displacement of about 3 m across a 90 m line next to the pier. Fig. 1a shows the location of the pier and the line used to measure the lateral displacement, while Fig. 1b displays the damaged pier due to the lateral displacement.

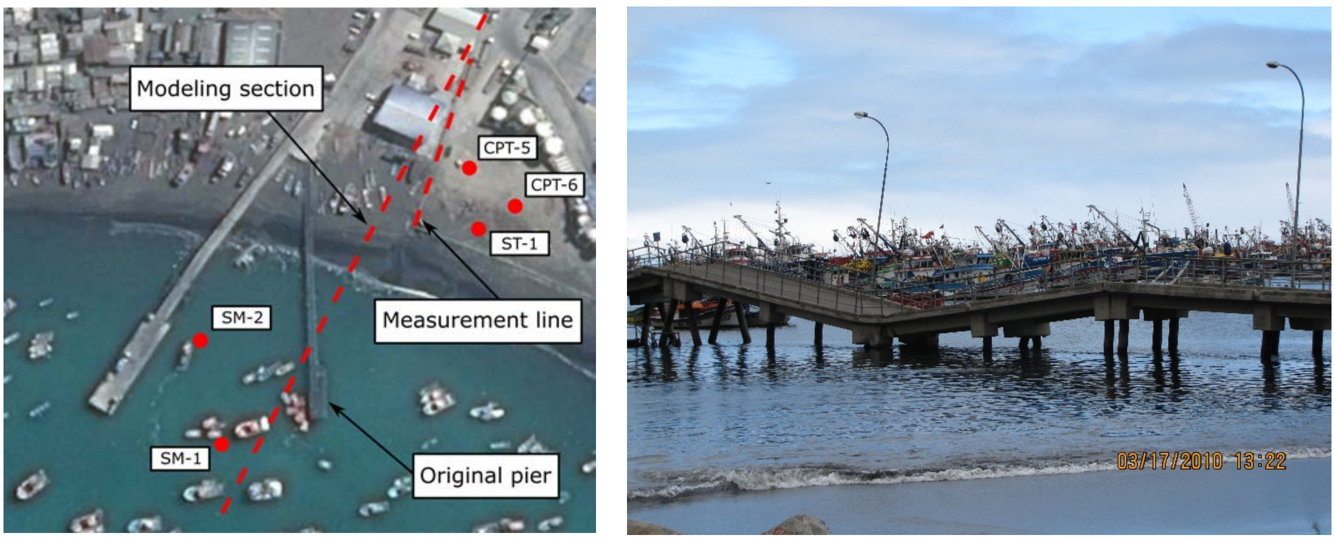

(a) (b)

Fig. 1 – (a) Port location, line of displacement measurement, and line of modeling section; (b) Collapsed pier due to liquefaction-induced lateral spreading.

To study the lateral spreading phenomenon and the seismic response of the pier during the earthquake, a FEM model was developed using the commercial software Plaxis 2D®. To represent the seismic response of the liquefiable layer, the constitutive model UBC3D-PLM [9], was used.

2. Geotechnical model

Close to the Lo Rojas site, an extensive exploration was performed to obtain soil samples and fully characterize the area. The exploration included CPTu soundings, SPT boreholes, and geophysical field tests. All the collected information was used to define a geotechnical profile of the site (details of this exploration can be found in [4]).

Fig. 1a shows the line section that was modelled, while Fig. 2 shows the developed geotechnical profile. As Fig. 2 shows, the soil at the zone is mainly composed by four units: (H1) poorly graded sand, (H2-H3) clayey sand and high plasticity clay, (H4) low plasticity clay, and, at the left bottom part of the model, a highly cemented soil.

The information gathered from the geotechnical exploration was also used to set up parameters for laboratory testing. The confining pressure and *in-situ* soil densities were estimated from CPTu data, while the moisture content, the specific gravity of the solids (G_s), the plasticity index (PI), and the grading curves of each soil were determined using borehole soil samples.

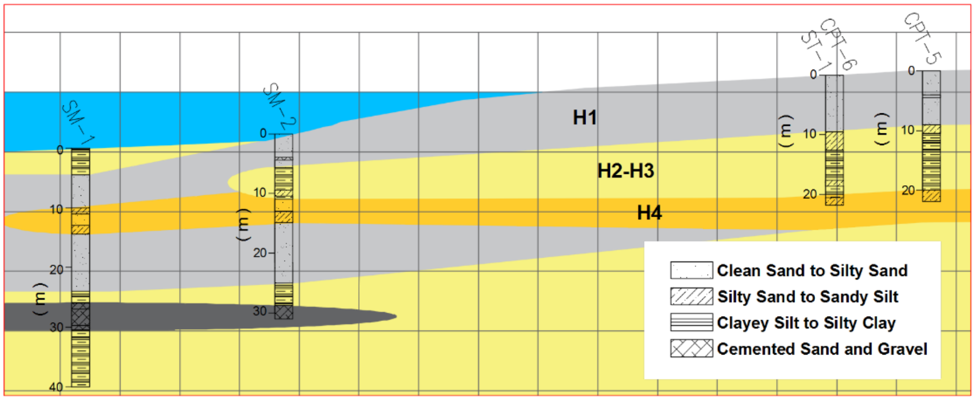

Fig. 2 – Geotechnical profile at Lo Rojas, Coronel (from [4]).

3. Laboratory tests

Several laboratory tests were conducted to obtain mechanical parameters for the soil layers at Lo Rojas fishermen area. All tests were performed on remolded samples. In the case of layers H4 and cemented soil, mechanical properties were estimated from SPT, geophysical field tests, and the literature.

3.1 Monotonic triaxial tests

To obtain the mechanical properties of the soil at Lo Rojas site, drained and undrained tests were carried out for materials of layers H1 and H2-H3.

In Fig. 3 the results of isotropically consolidated drained (ICD) and isotropically consolidated undrained (ICU) triaxial tests on soil samples of layer H1 are shown. All behavior curves obtained in laboratory were post-processed to obtain a first estimation of friction angle (ϕ') and cohesion (c') of each layer. Fig. 4 shows the results from the ICU tests on material H2-H3.

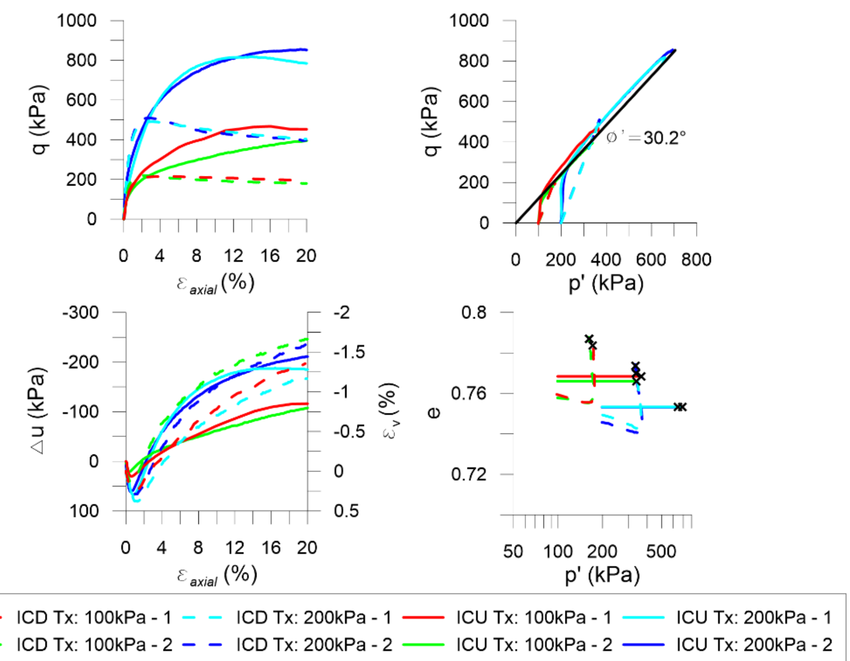

Fig. 3 – Monotonic ICU and ICD triaxial tests on H1 soil layer at confining pressures of 100 kPa and 200 kPa and a relative density of 30%.

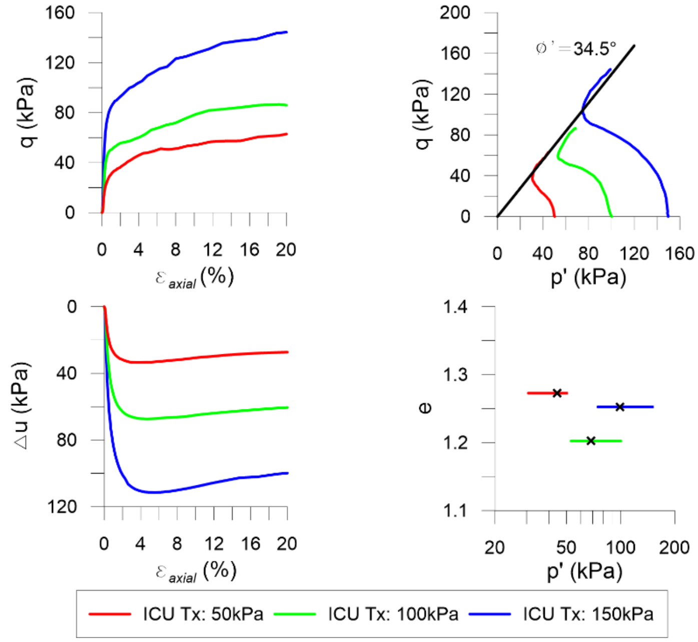

Fig. 4 – Monotonic ICU triaxial results from H2-H3 soil layer at confining pressures of 50, 100 and 150 kPa.

3.2 Resonant column and drained cyclic triaxial test

To analyze the drained cyclic behavior of the soils, a set of Resonant Column and Cyclic Triaxial tests were performed. These tests are used to characterize the stiffness degradation and damping curves of the materials.

Fig. 5 shows the shear modulus degradation and damping curves of soil layer H1. Results are compared against reference Toyoura sand results from [8]. It can be seen that, compared to Toyoura sand, Coronel sand (H1 soil) has a stiffer behavior up to 0.1% of cyclic strain, and it has less damping in the same deformation range.

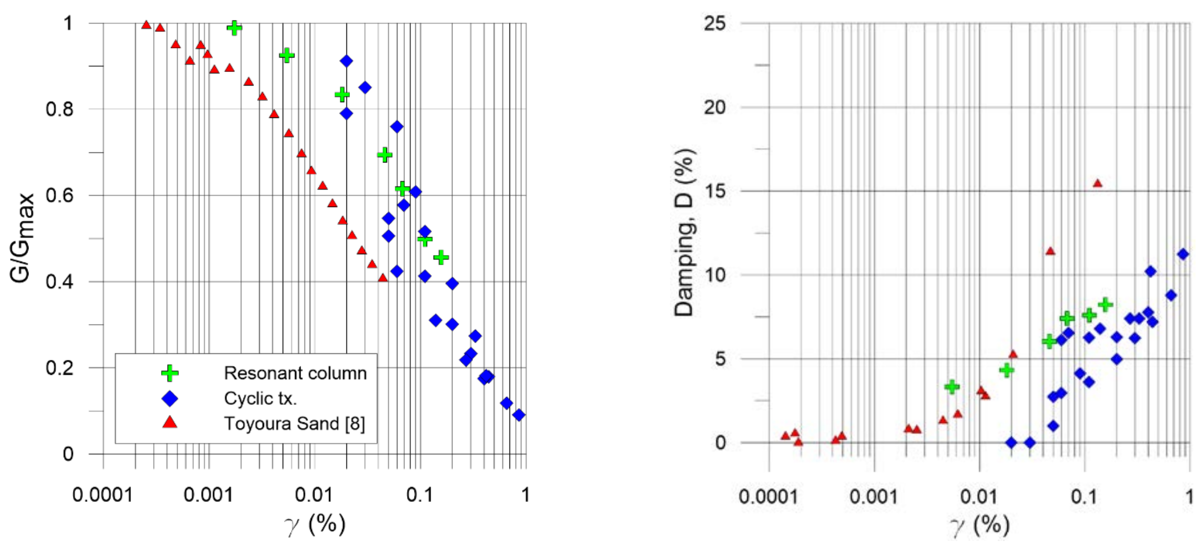

(a) (b)

Fig. 5 – (a) Shear modulus degradation curve of H1 soil layer at 100 kPa of confining pressure; (b) Damping curves of H1 soil layer at 100 kPa of confining pressure.

The shear wave velocity results obtained from cyclic laboratory test were approximately 130 m/s for H1 layer and 160 m/s for H2-H3 layer at 100 kPa of isotropic confinement. These values are in agreement with the geophysical field test results, where the V_{s15} parameter of two explored sites at Lo Rojas area were 150 m/s and 157 m/s [4].

3.3 Undrained cyclic triaxial tests

Cyclic undrained triaxial tests were used to characterize the liquefaction resistance of soils under cyclic stresses. Due to evidences of liquefaction of the H1 soil layer, a set of tests were performed at confining pressures of 100 and 200 kPa to obtain the liquefaction resistance curves.

Fig. 6 shows the liquefaction resistance curves. The cyclic stress ratio (CSR) is calculated as indicated in Eq. (1), where $\Delta\sigma_a$ is the axial stress deviator and σ'_{3c} is the isotropic consolidation stress. It can be seen that the curve for 200 kPa of confining pressure has a small reduction of resistance compared to 100 kPa curve because higher confinements make material more contractive during shearing.

$$CSR = \frac{\Delta\sigma_a}{2\sigma'_{3c}} \tag{1}$$

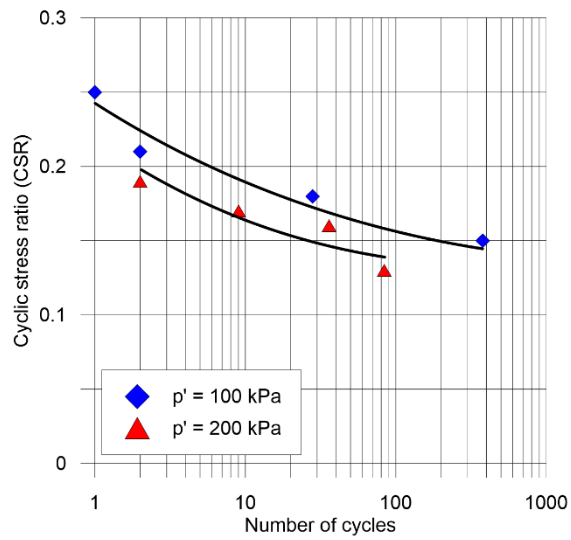

Fig. 6 – Liquefaction resistance curves for H1 soil layer at 100 kPa and 200 kPa of confining pressure.

4. Finite element model on Plaxis®

4.1 Model parameters

4.1.1 Soil

For materials H1 and H2-H3, parameters were obtained in two phases: (i) initial estimation of main parameters based on laboratory results, and (ii) using the Soil Test complement of Plaxis®, triaxial tests were simulated and secondary parameters were calibrated in accordance to the best fit with strain-stress paths from laboratory results.

In the case of H4 soil, the mechanical parameters were obtained from correlations [6], shear velocity profiles calculated by [4], and from damping and degradation curves from [12]. Because the cemented soil layer information is poor, it was assumed to be a soft rock or gravel and it was modelled using the Mohr-Coulomb constitutive model.

For the liquefiable soil (H1) two sets of parameters were calibrated: Hardening Soil model with Small Strain-Stiffness (HS-small), and UBC3D-PLM model. This last model needs the determination of two factors related to the densification rule (fac_{hard}) and to the post-liquefaction stiffness degradation of the soil (fac_{post}). These parameters were obtained by adjustment of liquefaction resistance curves of the model with laboratory results. For deepest H1 soil layer the same parameters as the shallow soil were used, but in that case, the $(N_1)_{60}$ parameter was selected according to SPTs soundings. The resulting set of fitted parameters is shown in Tables 1 to 3.

Table 1 – Calibrated HS-small properties of soil layers used in the model.

Parameter	Soil layer		
	H1	**H2-H3**	**H4**
Drainage type	Undrained A	Undrained A	Undrained B
Dry specific weight (kN/m^3)	15.55	12.00	15.50
Saturated specific weight (kN/m^3)	19.88	15.40	19.21
E_{50} (kN/m^2)	32.0e3	10.0e3	1.97e3
E_{oed} (kN/m^2)	32.0e3	16.0e3	1.58e3
E_{ur} (kN/m^2)	78.0e3	67.0e3	7.21e3
m (-)	0.50	0.50	1
ϕ'(°)	29.50	32.00	-
c' (kN/m^2)	0.00	0.00	-
S_u (kN/m^2)	-	-	150
ψ (°)	1.80	0.19	-
$\gamma_{0.7}$ (-)	0.38e-3	0.14e-3	0.22e-3
G_0 (kN/m^2)	32.88e3	43.94e3	28.40e3

Table 2 – Calibrated Mohr-Coulomb properties of the cemented soil layer used in the model.

Parameter	**Value**
Drainage type	Non porous
Dry specific weight (kN/m^3)	23.35
V_p (m/s^2)	1310
V_s (m/s^2)	700
ν (-)	0.30
ϕ'(°)	30
c' (kN/m^2)	0.00
ψ (°)	0.00

Table 3 – Calibrated UBC3D-PLM properties of liquefiable soil layer used in the model.

Parameter	**Value**
Drainage type	Undrained A
Dry specific weight (kN/m^3)	15.55
Saturated specific weight (kN/m^3)	19.88
ϕ'_{cv} (°)	30.2
ϕ'_{peak} (°)	32
c' (kN/m^2)	0
K_B^e	230
K_G^e	320
K_G^p	1750
m_e	0.5
n_e	0.5
n_p	0.4
R_f	0.9
fac_{hard}	0.2
$(N_1)_{60}$	5 to 30
fac_{post}	0.12

4.1.2 Pier structure

The pier structure consisted of steel pipe piles supporting a concrete slab. Modeling parameters were selected based on structural specifications of the original project. The port was mainly composed by two sections with different widths and transversal pile spacing. Tables 4 and 5 shows the piles and slabs properties.

Table 4 – Piles Properties.

Parameter	**Value**
Density (kN/m^3)	78.00
External diameter (m)	0.324
Profile thickness (m)	0.008
Young modulus (kN/m^2)	210e6
I (m^4)	9.872e-5

Table 5 – Slabs Properties.

Parameter	**Value**
Density (kN/m^3)	23.05
Thickness (m)	0.2
Transversal length (m)	4 to 6
Young modulus (kN/m^2)	2.57e7

Embedded pile row and plate elements were used to represent the longitudinal section of the port. However, because the real pier had a 3D orientation of piles, equivalent 2D flexural parameters must be chosen carefully. A 3D model on Plaxis® was used to iteratively calibrate the diameter and thickness of the equivalent 2D embedded pile row elements to obtain a similar behavior between 2D and 3D force-deformation curves of each line of piles.

The embedded pile elements were modeled with linear elastic elements, and the interaction between piles and the slab was considered rigid, transferring bending moments as well as shear and normal forces.

Embedded pile row elements need a maximum axial shaft resistance and a maximum base resistance for each pile. Those values were calculated using average values of SPT blow counts for each soil layer using the Aoki and Velloso method [11].

4.2 Model

To analyze the dynamic response to the Maule Mw 8.8 earthquake, two models were developed. First, a model without piles to obtain a reference estimation of soil response to cyclic loading, and to verify the ability of the model to reproduce field measurements. Second, a model that has the same geotechnical characteristics of the first model but with the pier structure included. In both cases the NS component of the Maule Mw 8.8 earthquake recorded at the Rapel station was selected to assess the seismic response of the model. This record was selected because the distance from Lo Rojas to the interplate fault is very similar to the distance from that plane to the Rapel station (see [4] for details).

4.2.1 Model without port structure

To obtain the site response, the model involves three major calculation phases:

- Initial phase: Initialization of stresses. This stage was simulated with gravity loading type to ensure the stress equilibrium in the model.
- Second phase: This phase includes the dynamic loading, and it has the same duration of the seismic signal.
- Third phase: To ensure the dissipation of the excess of pore pressures, a consolidation calculation was simulated. This phase has a simulated duration of one day.

Boundary conditions depend on the calculation phase. For the first and third phases, boundary conditions consisted on restrain movement in their normal boundary direction. For the second phase (dynamic), free-field elements (at the lateral limits of the model) and a compliant base (at the bottom of the model) were used.

Free-field boundaries are applied to incorporate the propagation of waves into the far-field. This effect is incorporated placing normal and tangential dashpots at each node of the lateral boundaries, where the parameters are selected from the soil closest to each dashpot. Compliant base boundary is designed to obtain a minimum reflection of waves at the base, and to input the ground motion.

Because the stiffness of dynamic boundaries is related to the neighboring soil properties at the beginning of the earthquake, those borders are not strong enough to fully contain the liquefied soil layer during the seismic movement. To avoid this effect, the geotechnical profile used to create the model had to be modified at the lateral boundaries. Two soil columns were added at each side: (i) 40 m wide inelastic soil column as a transition to free-field with the same properties of the original model, and (ii) 50 m wide columns composed of soil modeled with HS-small to represent the non-liquefiable far-field soil (Fig. 7).

The size of the mesh elements was selected according to [7], where it is recommended that the average size cannot be greater than one-eighth of the wavelength associated to the maximum frequency with significant energy content of the seismic signal. From the Fourier amplitude spectrum, the greater frequency with significant energy content was around 10 Hz, and from the geophysical field tests the lower shear wave velocity was between 120 and 130 m/s. Using this data, a maximum average size of 1.5 to 1.6 m was selected for the elements of the model. The model without the pier structure is composed of 11,633 triangular 15-node elements, and it has an average element size of 1.6 m.

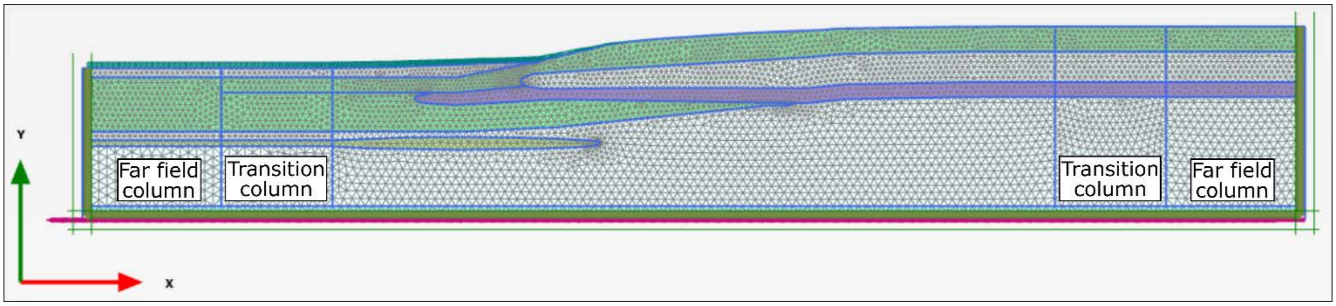

Fig. 7 – Finite element mesh used in Plaxis 2D® to model Lo Rojas location without port.

4.2.2 Model with pier

In this model, the boundaries and geotechnical materials are those of the previous model. To incorporate the pier, embedded pile row and plates elements were used. The calculation phases for this simulation are the same as the original model, but a plastic calculation stage is added between the initial and the dynamic phases to include the initial stresses generated by the pier structure. The other phases remain identical, but in the dynamic and in the consolidation analysis, the structure is also activated. The generated finite-element mesh is shown in Fig. 8. It is composed of 11,810 elements with an average size of 1.6 m.

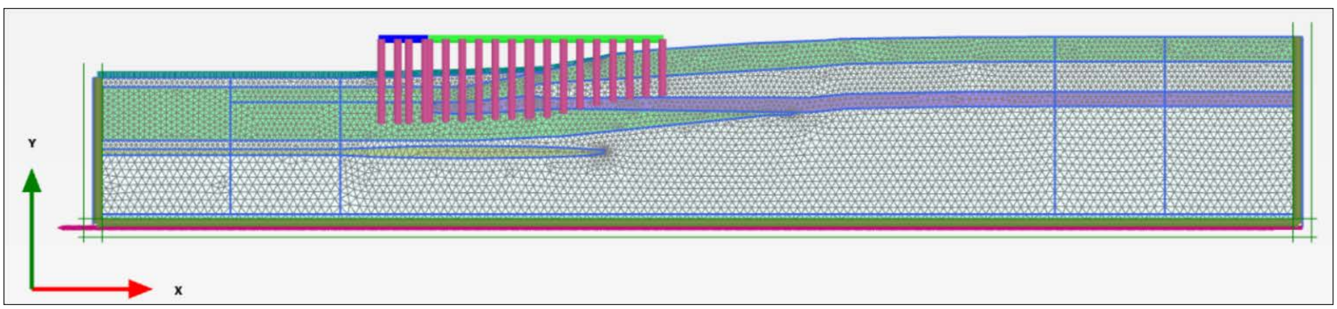

Fig. 8 – Finite element mesh used in Plaxis 2D® to model Lo Rojas location including the port.

4. Model results

Computed horizontal relative displacements across the measurement line (see Fig.1a) are shown in Fig. 9. As it can be seen, the obtained maximum horizontal displacements are similar to those measured during the post-earthquake survey [3]. The cumulated lateral movement across the measurement line is about 2.8 m in both models. As expected, due to the pile-pinning effect, when piles are included in the model lateral displacement tend to diminish.

Simulation results show a variable lateral deformation rate. The computed deformation rate in the 40 m closest to the wall face is 10 times larger than that of more distant points. In addition, close to the wall face, the measured deformation is similar to those computed by the model. The general tendency is reasonably reproduced and we believe that the model can provide realistic values of internal forces and displacement demand on the piles.

Due to seismic amplification, peak accelerations increase from 0.19 g at the model base to 0.20 to 0.50 g at the model surface. Because there is no earthquake record close to the study site with similar geotechnical conditions, those values cannot be directly compared to the accelerations recorded at other sites. The highest PGA values are located 30 to 40 m from the pier and they occur prior to full liquefaction of the shallow layer of soil.

The sensitivity of the results on the input motion is under study, nevertheless as [4] shows, the results of lateral spread for the Rapel record without pier are approximately the mean value when other available rock input motions from the Maule 2010 event are considered. We believe that a similar tendency will be found when the pier is included in the model.

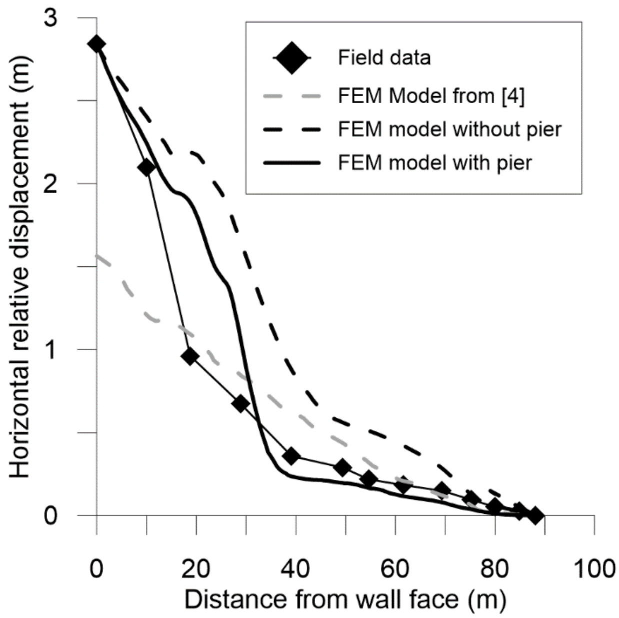

Fig. 9 – Model results of superficial displacement.

Fig. 10 shows the obtained horizontal displacement contours. The accumulated horizontal displacements at the end of the earthquake are concentrated at the side of the port closer to the shore, with a maximum lateral deformation of 3.5 m. As this figure shows, soil tends to form a wedge in the shallow buried zone of the piles placed in the more inclined area, moving this part of the structure to the ocean and pushing the rest of the pier. Post-earthquake horizontal displacements are around 1 to 1.7 m at the ground surface in the pier area, while at the bottom part of the structure they are approximately 0.1 to 0.5 m. Additionally, as shallow liquefied material moves more than the deeper soils, significant bending is induced in the pile elements (Fig. 12).

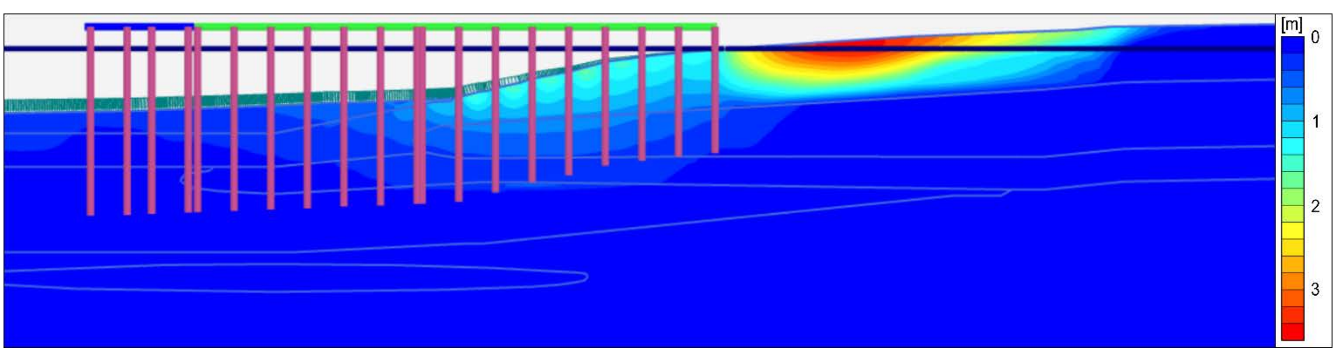

Fig. 10 – Soil horizontal displacements.

As mentioned before, the pier was composed by piles and a concrete slab (divided into three sections). Plates (in green on Fig. 10) have 2.5 m of out-of-plane width, while the one displayed in blue has 4.5 m of out-of-plane width. Horizontal displacements of the pier slabs varied between 0.35 m and 1.4 m, while vertical downward displacement oscillated between 0.01 m and 0.2 m. The maximum deformation values were obtained in the part of the structure located at the steepest ground surface. At this place, the first pile of the pier has a rotational component of about 3.5° (Fig. 11).

The post-earthquake survey at Lo Rojas [3] describes the deformed structure shape as the landward part moved to the ocean compressing the pier against the seaward end. This structural response caused the seaward end to "raise" relatively to the rest of the pier. As Fig. 11 shows, the model results have the same qualitative deformed shape at the end of the seismic motion. However, the model is unable to capture piles' interaction when they get in contact as the deformation increase.

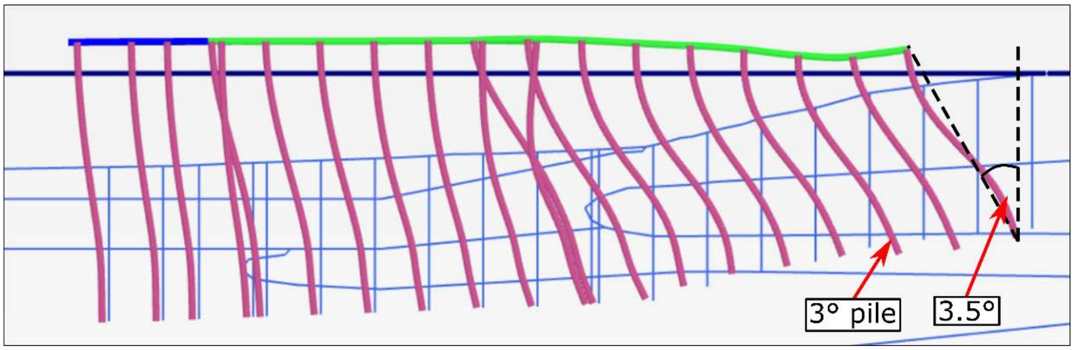

Fig. 11 – Post-seismic deformation of the pier (augmented 10 times).

Fig. 12 shows the envelops of seismically induced internal shear ($Q_{seismic}$) and bending moment ($M_{seismic}$) of the third pile from the seashore to the ocean (Fig. 11). In the case of shear forces, the diagrams show the effect of the shallow liquefiable soil thrust pushing to left, while close to end of the pile, a reaction equilibrates this lateral force. Regarding the bending moment diagram, there are three critical sections with similar high values: (i) the slab-pile connection, (ii) below the ground level in the liquefied layer, and (iii) close to the interface of the shallow material and the non-liquefiable layer. Those zones are critical to design the structure, because the first one was the location of several sources of failure observed in the structure. The nominal yielding bending moment of the piles is about 142 kN-m. This value is less than the maximum applied moment, indicating that the pile already reached the yield strength in FEM results.

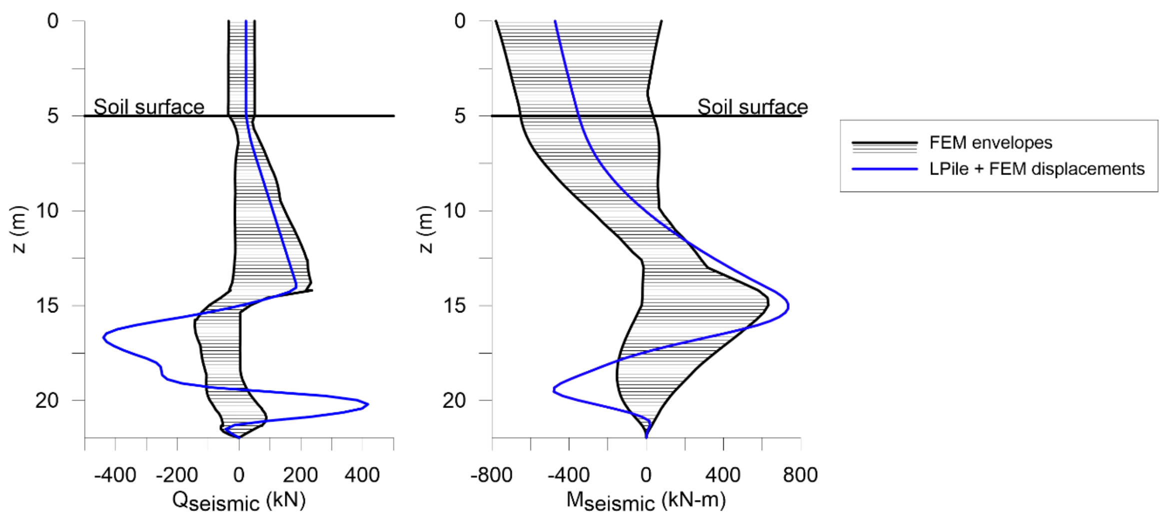

Fig. 12 – Dynamic internal force envelops for the third pile from the shore to the ocean.

Shear and bending moment diagrams obtained from the FEM model were compared against a simplified method to calculate the lateral spreading effects over piles. Methods based on liquefaction resistance factor, as those described in [1], were not applicable to this case, because of the analytical lateral displacement achieved were not realistic for the site characteristics. An approximation using LPile® software and model results was conducted imposing the liquefied state using soil displacements of FEM model in free field case (without the structure). To include the inertial effect of the concrete slab, a shear force, equal to the product of the tributary mass and the maximum slab acceleration, was added at the top of the pile.

As Fig. 12 shows, the resultant internal forces from LPile® analysis are, in general, contained by the envelops of shear and bending moment from Plaxis®. The shapes of the curves are relatively similar and agree with the soil behavior in liquefied state. However, there are differences between the maximum values and their location. In the case of the shear force, the simplified model predicts a maximum value of more than two times that of the FEM model, and it takes place at a different location.

5. Conclusions

The main conclusions of this study are:

- Plaxis® software is able to properly represent the seismic soil response of the liquefiable materials. As Fig. 9 shows, the response along the field measurement line was satisfactorily reproduced by the developed FEM model.
- Horizontal relative displacements predicted by Plaxis® are greater than field observations at points close to the reference wall. This could be related to the soil layer simulated using UBC3D-PLM. This layer liquefies earlier than real soil, hence the post-liquefied behavior predicted by the model is less rigid than the actual behavior of soil.
- Due to the 3D nature of the modeled port, results of 2D model are only an approximation of the real problem. Two dimensional model enforces a plane-strain condition modifying the loading transfer between the piles and the surrounding soil, which does not include three dimensional topography/bathymetry and soil variability influence, and it cannot simulate the complete three-component seismic loading. More realistic results could be, in principle, achieved with a 3D model incorporating all the features mentioned above. Nevertheless, simulated residual 2D deformations of the pier are very similar to the available damage description from the post-earthquake survey.

5. References

[1] Ashford S.A., Boulanger R.W., Brandenberg S.J. (2011). Recommended design practice for pile foundations in laterally spreading ground. PEER report 2011/04, Pacific Earthquake Engineering Research Center. University of California, Berkeley.

[2] Bardet J.P. (1997). *Experimental soil mechanics*. Prentice Hall.

[3] Bray J., Rollins K., Hutchinson T., Verdugo R., Ledezma C., Mylonakis G., Assimaki D., Montalva G., Arduino P., Olson S.M., Kayen R., Hashash Y., Candia G. (2012). Effects of ground failure on buildings, ports, and industrial facilities. *Earthquake Spectra*, **28** (S1), S97-S118.

[4] De la Maza G., Williams N., Sáez E., Rollins K., Ledezma C. (2016). Liquefaction-induced lateral spread in Lo Rojas, Coronel, Chile. Field study and numerical modeling. *Earthquake Spectra*, **in press**.

[5] Departamento de ingeniería Civil Universidad de Chile (2012). *Mw=8.8 terremoto en Chile, 27 de febrero 2010.*

[6] Kulhawy F.H., Mayne P.W. (1990). Manual on estimating soil properties for foundation design. United States.

[7] Laera A., Brinkgreve R.B.J. (2015). Site response analysis and liquefaction evaluation.

[8] Lo Presti D.C.F., Pedroni S., Cavallaro A., Jamiolkowski M., Pallara O. (1997). Shear modulus and damping of soils. *Géotechnique*, **47** (3), 603-617.

[9] Petalas A., Galavi V. (2013). Plaxis liquefaction model UBC3D-PLM.

[10] Plaxis 2-D (2015). Reference Manual.

[11] Salgado R., Lee J. (1999). Pile design based on cone penetration test results. FHWA/IN/JTRP-99/8, Purdue University, West Lafayette, IN.

[12] Vucetic M., Dobry R. (1991). Effect of soil plasticity on cyclic response. *Journal of Geotechnical Engineering*, **117** (1), 89-107.